8 HIGHLIGHT OF THE MONTH

Forces and Lattice Relaxations Calculated by a Full-Potential KKR-Green's Function Method

T. Korhonen, N. Papanikolaou, R. Zeller, and P. H. Dederichs
Institut für Festkörperforschung, Forschungszentrum Jülich, D-52425 Jülich, Germany

N. Stefanou
University of Athens, Section of Solid State Physics, Panepistimioupolis, GR-15784 Athens, Greece

Abstract

In this review we demonstrate that a recently developed full-potential KKR-Green's function method allows an efficient calculation of forces and lattice relaxations in transition metals. The forces can be readily evaluated by the ionic Hellmann-Feynman theorem, while the Green's functions for shifted positions can be obtained by angular momentum transformations. As applications we calculate the lattice relaxations around impurities in Cu and Al. Moreover, we show that the method allows to determine the phonon frequencies of transition metals from a single self-consistent calculation of the coupling constants in real space and present results for ferromagnetic Ni.

8.1 Introduction

The KKR method of electronic structure calculations, introduced by Korringa [1] and Kohn and Rostoker [2], is well known for its mathematical rigorousness and elegance. By taking advantage of multiple scattering theory, the method clearly separates the scattering properties of the single potentials from the geometrical structure of the system. Moreover, the size of the resulting algebraic equations is optimally small. On the other hand, the KKR theory is subtle and complex, so that even the evaluation of the free-space structure constants represents a problem in itself. Moreover, its numerical implementation for band-structure calculation is neither easy nor efficient. This has lead to the fact that the linear methods, like LMTO, ASW, and LAPW, received over the years considerably more attention.

The Green's function (GF) version of the KKR method was introduced by Beeby and others [3, 4, 5] and has later-on been used by the authors in extensive calculations for impurities in metals [6, 7, 8]. The GF version is particularly useful for density-functional calculations and avoids part of the disadvantages connected with the band-structure problem. For instance, the integration over all occupied states can be efficiently performed by a contour integration in the complex energy plane, so that for ground state calculations the time consuming evaluation of the eigenvalues is avoided. Moreover, the availability of the Green's function opens up the way to applications like linear-response problems, disorder in alloys, e.g., within the CPA, and electronic transport in solids [9].

Unfortunately, most KKR calculations up to now have been restricted to spherical potentials of muffin-tin or ASA form. This is a serious limitation of the theory since the structural optimization of a system requires a full-potential description. In this highlight we will review our recent work on extending the KKR-GF method into a full-potential scheme and then show that this allows an accurate and efficient calculation of forces and lattice relaxations. The applicability of full-potential KKR schemes has been widely discussed in the literature [10, 11, 12, 13, 14, 15, 16] and in the view of most authors, this is simply a question of the convergence of the angular momentum expansion which may differ in different versions of the full-potential KKR theory. In view of our experience with the calculated results described below the convergence of the full-potential KKR-GF method described in section 8.2 seems not to be a problem in practical calculations. In contrast to most other methods, the force calculation is very easy within the KKR formalism, while the description of lattice relaxation is more complicated. One should also note that the KKR theory is very different from methods based on localized or mixed orbitals. For instance, the overlap between orbitals on neighboring sites does not enter at all nor has an interstitial region to be introduced. Instead, the solutions in each cell are constructed by angular momentum expansions, and the proper boundary conditions are satisfied by the solution of the Dyson equation.

The outline of the paper is as follows: First we shortly describe the full-potential extension of the KKR formalism in Sec. 8.2 and sketch the calculation of forces and lattice displacements in Sec. 8.3. We then present results for the lattice relaxations around impurities in metals (Sec. 8.4) and demonstrate that the same method can also be used to calculate phonons in real space (Sec. 8.5). Finally we conclude this highlight with a short summary and an outlook on further developments of the KKR method.

8.2 Full-Potential KKR-Green's Function Method

In the sense of multiple-scattering theory, the whole space is divided into non-overlapping and space-filling cells around each atomic site $\mathbf{R}^n$. The crystal Green's function, G, is then written in a cell-centered double expansion around the positions $\mathbf{R}^n$ and $\mathbf{R}^{n'}$ in different cells as [7]

$$G(\mathbf{r}+\mathbf{R}^n,\mathbf{r}'+\mathbf{R}^{n'};E) = \delta_{nn'}G_s^n(\mathbf{r},\mathbf{r}';E) + \sum_{L,L'} R_L^n(\mathbf{r};E)G_{LL'}^{nn'}(E)R_{L'}^{n'}(\mathbf{r}';E) \ , \qquad (2)$$

where $G_s^n(\mathbf{r},\mathbf{r}';E)$ represents the Green's function for a single potential confined inside the cell n in otherwise free space. In the above equation, the position vectors $\mathbf{r}$ and $\mathbf{r}'$ are restricted to the Wigner-Seitz cell and the index L denotes the angular momentum quantum numbers (ℓ,m).

The partial wave $R_L^n(\mathbf{r};E)$ is defined to be the solution of the Lippmann-Schwinger equation for a spherical wave $j_\ell(r\sqrt{E})Y_L(\hat{\mathbf{r}})$ incident on the potential $V^n(\mathbf{r})$ at the site $\mathbf{R}^n$

$$R_L^n(\mathbf{r};E) = j_\ell(r\sqrt{E})Y_L(\hat{\mathbf{r}}) + \int d\mathbf{r}'\, g(\mathbf{r},\mathbf{r}';E)V^n(\mathbf{r}')R_L^n(\mathbf{r};E)\ . \tag{3}$$

Here r is the length of the vector $\mathbf{r}$ and j_ℓ and Y_L are the spherical Bessel functions and the spherical harmonics, respectively, while $g(\mathbf{r},\mathbf{r}';E)$ is the free-electron Green's function being analytically known. In our full-potential KKR-GF method, the potentials and the partial waves are expanded in real spherical harmonics as

$$V^n(\mathbf{r}) = \sum_L V_L^n(r)Y_L(\hat{\mathbf{r}}) \tag{4}$$

and

$$R_L^n(\mathbf{r};E) = \sum_{L'} R_{L,L'}^n(r;E)Y_L(\hat{\mathbf{r}})\ . \tag{5}$$

The non-spherical part of the potential, $\Delta V^n(\mathbf{r}) = V^n(\mathbf{r}) - V_0^n(r)$, couples the angular momentum channels and leads to a system of coupled radial equations for the functions $R_{L,L'}^n$. These equations can be solved quite efficiently by the following procedure: First, calculate the solutions $R_\ell(r;E)$ corresponding to the spherical part of the potential, $V_0^n(r)$, and then calculate the full solutions iteratively by using an integral equation with $\Delta V^n(\mathbf{r})$ as perturbative potential. The corresponding Born series converges rapidly, and in most cases the second Born approximation is already sufficient for an accurate solution to the coupled radial equations [17].

When solving the radial and Poisson equations, the shape of the different cells is described by the shape functions $\Theta^n(\mathbf{r})$, being equal to 1 inside the cell n and vanishing everywhere else. These functions are also expanded in real spherical harmonics as

$$\Theta^n(\mathbf{r}) = \sum_L \Theta_L^n(r)Y_L(\hat{\mathbf{r}})\ . \tag{6}$$

The (possibly) distorted lattice is described in this work by keeping the same space division as in the undistorted lattice, but the shape functions are expanded around the shifted atomic positions. This procedure is working well for small displacements. For larger displacements, the use of the Wigner-Seitz construction in the distorted geometry would be a better choice to obtain the cells because it optimizes the angular momentum convergence of the wave functions.

While the ℓ-convergence of the expansion (6) is rather slow, the overall convergence is determined by the ℓ-cut-off of the wave functions $R_{L,L'}^n$ of Eq. (5). If here angular momenta up to $\ell_{\max}$ are taken into account, then the expansion of the charge density and the potential (Eq. 4) includes only contributions up to $2\ell_{\max}$, while the evaluation of the Coulomb and exchange-correlation terms in the potential energy requires ℓ-terms up to $4\ell_{\max}$. Thus only shape functions $\Theta_L^n(r)$ up to $4\ell_{\max}$ are needed in the calculations.

The multiple scattering is contained in the second term of Eq. (2) through the so-called structural Green's function $G_{LL'}^{nn'}(E)$. This can be obtained by the Dyson equation

$$G_{LL'}^{nn'}(E) = G_{LL'}^{0,nn'}(E) + \sum_{n''L''L'''} G_{LL''}^{0,nn''}(E)\Delta t_{L''L'''}^{n''}(E)G_{L'''L'}^{n''n'}(E)\ , \tag{7}$$

which can be written in matrix notation as

$$\mathcal{G} = \mathcal{G}^0 + \mathcal{G}^0\Delta\mathrm{t}\mathcal{G}\ , \tag{8}$$

where $\mathcal{G}^0$ is the structural Green's function of the reference system and $\Delta\mathsf{t} = \mathsf{t} - \mathsf{t}^0$ is the difference between the site-diagonal t-matrices of the reference and the actual systems. The latter one is given by

$$t^n_{LL'}(E) = \int d\mathbf{r}\, j_\ell(r\sqrt{E}) Y_L(\hat{\mathbf{r}}) V^n(\mathbf{r}) R^n_{L'}(\mathbf{r}; E) \ . \tag{9}$$

In the Dyson equation the non-spherical character of the full potentials $V^n(\mathbf{r})$ enters only in the non-diagonal elements $t^n_{LL'}$ of the t-matrix. From numerical point of view, they present no complication and no increase in computer time occurs in the solution of the Dyson equation. Thus only the single-site scattering problem, in particular the solution of the coupled radial equations, becomes more complicated. Therefore, the additional numerical effort needed for the full-potential KKR calculations compared to the muffin-tin KKR calculations scales only linearly with the number of non-equivalent potentials.

The electron density in cell n can be calculated from the imaginary parts of the site-diagonal elements of the Green's function

$$n^n(\mathbf{r}) = -\frac{1}{\pi} \int_{E_B}^{E_F} dE\, \mathrm{Im}\{ G(\mathbf{r} + \mathbf{R}^n, \mathbf{r} + \mathbf{R}^n; E)\} \ . \tag{10}$$

Here, the energy integral extends over all occupied states from a suitably chosen energy, E_B, between the valence band and the core states up to the Fermi energy, E_F. By using analytical properties of the Green's function, one can replace the energy integration in Eq. (10) by a contour integral in the complex energy plane, which can be evaluated with much fewer energy points. In this case, the full structure of the Green's function close to E_F is important, so that the energy mesh has to be more dense in this region. A recent extension to finite temperatures, using a Fermi-Dirac distribution for the occupation function, has the additional advantage that only complex energies are needed. The closest one to the real axis is given by $E_F + i\pi kT$, the value of the first Matsubara energy [18].

8.3 Calculation of Forces and Lattice Relaxations

From the self-consistent charge densities and potentials, one can calculate the forces on the atoms by using an ionic version of the Hellmann-Feynman theorem [19]

$$\mathbf{F}^n = Z^n \left. \frac{\partial V^n_C(\mathbf{r})}{\partial \mathbf{r}} \right|_{\mathbf{r}=\mathbf{0}} - \int d\mathbf{r}\, \rho^n_c(r) \frac{\partial V^n_{\mathrm{eff}}(\mathbf{r})}{\partial \mathbf{r}} \ , \tag{11}$$

where $V^n_C(\mathbf{r})$ is the Coulomb part of the effective one-electron potential, $V^n_{\mathrm{eff}}(\mathbf{r})$, in cell n due to all electrons and all other nuclei outside this cell. Clearly, the first term is the force on the nucleus, evaluated with spherical core charge densities, $\rho^n_c(r)$, and the second term is the force on the core electrons. It is obvious that the force on the nucleus is to a large extent compensated by a nearly equal but opposite force on the core electrons. In deriving the ionic force formula (11), it is only assumed that the unperturbed core density is spherically symmetric. Therefore, the force formula is equally valid if one makes the frozen core approximation or if the core states are allowed to relax retaining the spherical symmetry as it is usually done in all-electron calculations. Within the full-potential KKR-GF method, the force calculation does not require an additional effort, since the force is readily calculated from the $\ell = 1$ components of the

potentials and since all potential components are anyhow evaluated up to $2\ell_{\max}$ self-consistently. As a further advantage of the KKR theory, Pulay corrections to the force formula (11) arising from the restriction to a finite basis set vanish within the formalism so that in the full-potential description the evaluation of the force is straightforward.

Compared to this the evaluation of lattice relaxations becomes more complicated. This is due to the fact that one needs two angular momentum expansions, one for the unshifted ("ideal") position and one for the new shifted position. While the Green's function for such "interstitial" positions can also be evaluated by Brillouin zone integration, we use here a simpler method introduced by Lodder [20] which is, however, limited to small displacements. The structural Green's function $\mathcal{G}^0 = \{G^{0,nn'}_{LL'}\}$ of the host transformed to the shifted positions $\mathbf{R}^n + \mathbf{s}^n$ and $\mathbf{R}^{n'} + \mathbf{s}^{n'}$ is given by

$$\tilde{\mathcal{G}}^0 = \mathcal{U}\mathcal{G}^0\mathcal{U}^{-1} \ , \tag{12}$$

where the transformation matrix $\mathcal{U}$ is local in the site index and given by

$$U_{LL'}(\mathbf{s}^n) = 4\pi \sum_{L''} i^{\ell''-\ell'+\ell} C_{LL'L''} j_{\ell''}(s\sqrt{E}) Y_{L''}(\hat{\mathbf{s}}^n) \ , \tag{13}$$

where $C_{LL'L''}$ are the Gaunt coefficients and s is the length of the displacement vector $\mathbf{s}^n$. From the behavior of the Bessel functions for small arguments it can be seen, that for small displacements contributions arising from $\ell'' > 1$ can be neglected and that the matrix $\mathcal{U}$ couples angular momentum quantum numbers ℓ with $\ell \pm 1$, so one has to increase the angular momentum cut-off of the radial wave functions, e.g., from $\ell_{\max} = 3$ to $\ell_{\max} = 4$. An analogous expression holds for the unshifted t-matrix ,t^0, of the host in the shifted ℓ-representation, i.e., $\tilde{\mathrm{t}}^0 = \mathcal{U}\mathrm{t}^0\mathcal{U}^{-1}$, so that in the shifted representation the Dyson equation takes the form

$$\mathcal{G} = \tilde{\mathcal{G}}^0 + \tilde{\mathcal{G}}^0(\mathrm{t} - \tilde{\mathrm{t}}^0)\mathcal{G} \ , \tag{14}$$

which is quite analogous to Eq. (8) except for the complications arising from the $\mathcal{U}$-transformation and the resulting increase in $\ell_{\max}$.

In order to accelerate the determination of the equilibrium atomic positions from the *ab initio* forces, we use a lattice statics simulation based on the Kanzaki method [21]. In the harmonic approximation the displacement pattern $\mathbf{s}^{n'}$ is related to the force distribution, $\mathbf{F}^n$, by $\mathbf{F}^n = \sum_{n'} \Phi^{nn'}\mathbf{s}^{n'}$, where Φ denotes the coupling constant matrix of the defect system. By splitting this up, $\Phi = \Phi_0 + \Delta\Phi$, into the coupling constant matrix Φ_0 of the ideal crystal and the changes $\Delta\Phi$ induced by the defect, the Kanzaki forces are given by

$$\mathbf{F}^n_K = \sum_{n'} \Phi^{nn'}_0 \mathbf{s}^{n'} = \mathbf{F}^n - \sum_{n'} (\Delta\Phi)^{nn'}\mathbf{s}^{n'} \ , \tag{15}$$

In the simulation we use for the Born-von Karman parameters, Φ_0, values fitted to experimental phonon dispersion curves (they might as well be calculated; see below). The changes $\Delta\Phi$ are restricted to the first nearest neighbors of the defect and determined from *ab initio* calculations where only these first nearest neighbors are moved. The force pattern $\mathbf{F}^n_K$ is then applied on a hypothetical ideal lattice described by coupling constants Φ_0 and the displacements of all atoms are determined self-consistently. The resulting $\mathbf{s}^n$ are used as input in the next *ab initio* study and the whole procedure is repeated until all forces $\mathbf{F}^n$ are sufficiently small. Usually, one or

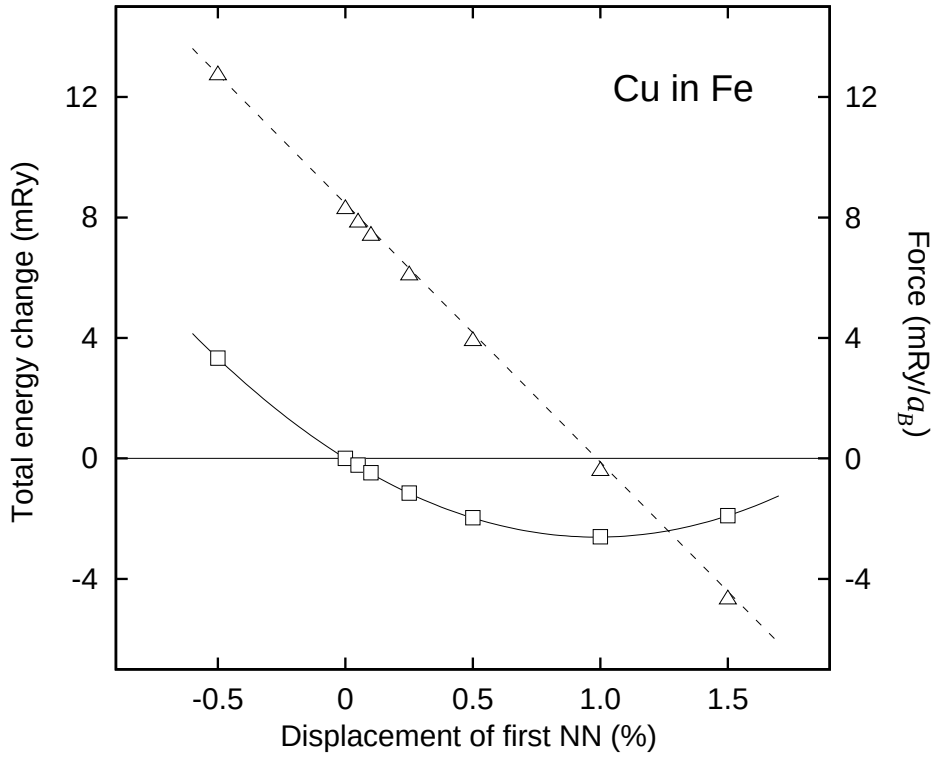

Figure 1: Total energy variation and radial force on a first nearest neighbor (NN) atom as a function of the change of the NN distance for a Cu impurity in bcc Fe. The dashed line shows the resulting force as obtained from a parabolic fit (solid line) to the calculated total energies (squares). The triangles are the *ab initio* forces calculated from the Hellmann-Feynman theorem (11).

two such iterations are enough. The Kanzaki forces $\mathbf{F}_K^n$ determined in this way can be used to determine the volume change ΔV induced by the defect, which can be experimentally obtained from lattice parameter measurements. The volume change is given in the Kanzaki model as

$$\Delta V = \frac{1}{3K} \sum_n \mathbf{F}_K^n \cdot \mathbf{R}^n \ , \tag{16}$$

where K is the bulk modulus of the ideal crystal.

To demonstrate the accuracy of the force calculation we discuss the relaxation of the first nearest neighbors for a Cu impurity in bcc Fe. Fig. 1 shows the variation of the total energy, if only the first nearest neighbor (NN) atoms are shifted. The dashed line shows the resulting force as obtained from a parabolic fit (solid line) to the calculated total energy values (squares) which compares very well with the *ab initio* forces (triangles) from the Hellmann-Feynman theorem (11). In both cases an outward relaxation of 1 % of the NN distance is obtained. The slope of the force curves can be used to determine the change $\Delta\Phi$ of the coupling parameters in Eq. (15).

8.4 Lattice Displacements around Impurities

We have performed calculations of lattice displacements around impurities in Al and Cu. The calculations were done using a cluster of 79 perturbed potential, so that an impurity and the 5

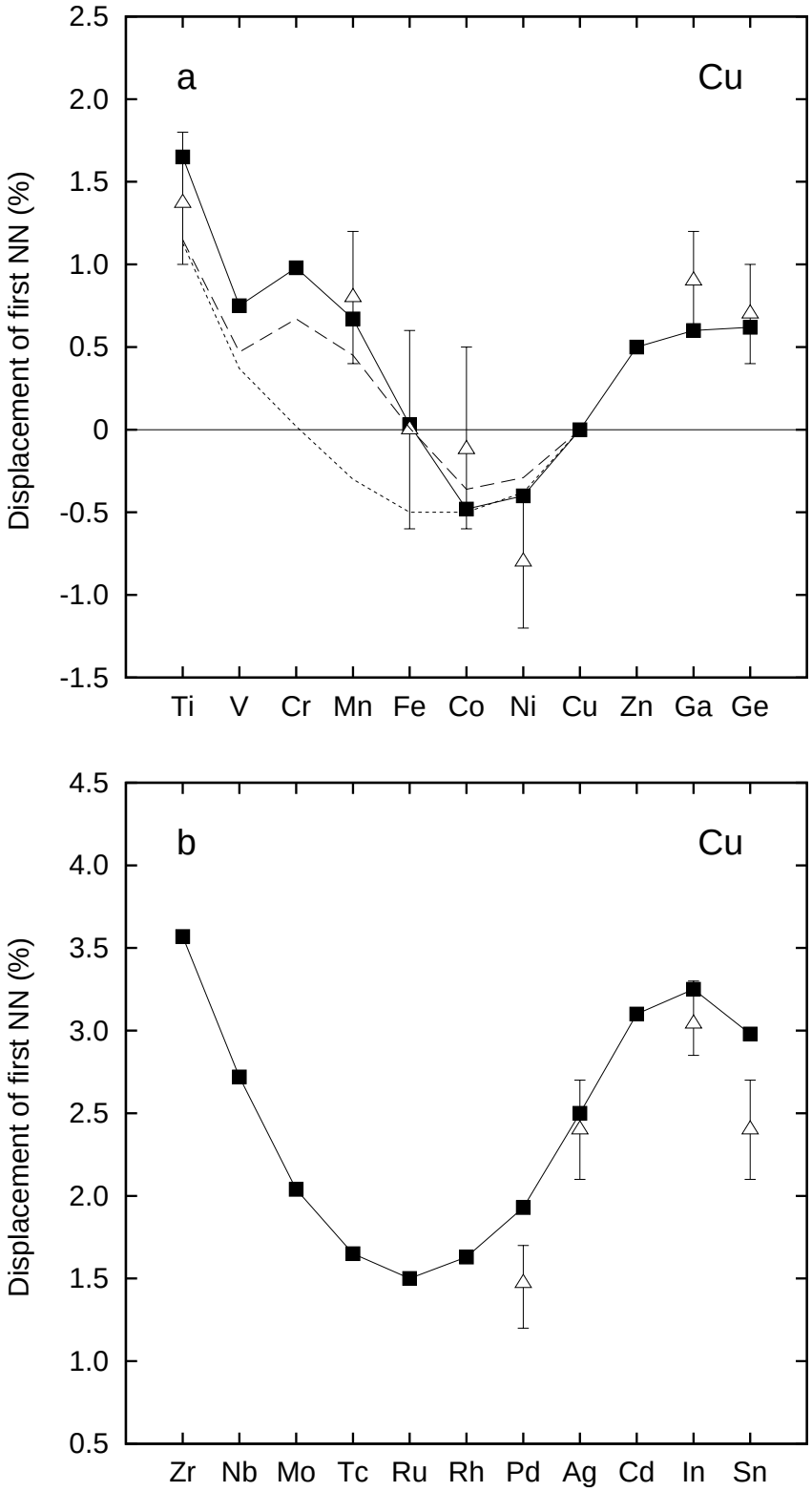

Figure 2: Calculated (solid squares) and experimental (open triangles with error bars) first NN shifts around 3d and 4sp (a) and around 4d and 5sp (b) substitutional impurities in Cu. The experimental values are the EXAFS data from Ref. [22]. Dashed and dotted lines are the results of calculations allowing only first NN relaxation for spin-polarized and non-spin-polarized cases, respectively.

NN fcc shells around the impurity were treated self-consistently. The theoretical values for the lattice constants obtained by a total energy minimization were used in both cases. The values 7.55 a.u. and 6.71 a.u. for Al and Cu, respectively, are somewhat smaller than the corresponding experimental values 7.65 and 6.82 a.u., representing a known failure of the LDA.

Fig. 2 shows the calculations of the first NN relaxations for a large number of impurities in Cu, i.e., for impurities of the 3d and 4sp series in Fig. 2a and of the 4d and 5sp series in Fig. 2b. The calculated values as given by the solid squares are in excellent agreement with EXAFS data of Scheuer and Lengeler [22]. The dashed line refers to a calculation where only the n.n. atoms were allowed to relax and all other atoms were fixed. This always underestimates the relaxation of the nearest neighbors.

As can be seen from Fig. 2, most impurities dilate the Cu lattice. Due to their large atomic sizes, this is particularly true for the 4d and 5sp impurities. The parabolic behavior across the 4d series is quite analogous to the behavior of the lattice constants of the 4d metals and can be explained by simple band filling arguments. In the 3d series the behavior is more complicated due to magnetism. While a non-spin-polarized calculation (dotted line) leads also to a parabolic trend, the large local moments of the Cr, Mn, and Fe impurities give rise to a pronounced magneto-volume expansion which also shows up in the EXAFS experiments. While the local moments strongly affect the lattice relaxations, the opposite is not true: The local moments are quite stable in Cu and are barely affected by the relaxation. For instance, the Mn-moment increases slightly from 3.39 μ_B to 3.42 μ_B when changing from the unrelaxed configuration to the relaxed one.

The calculations show that for the early 3d and 4d impurities in Cu a realistic description of the relaxations is only obtained, if the semicore s- and p-states are treated as valence states. For instance, for Ti or Zr impurity the first NN relaxations would be 50 or 60 % too large, if the semicore states were treated as core states. Therefore, we use in our calculations an extra long energy contour which includes both the valence states as well as the semicore states of the impurity. Thus contrary to the linearized methods the full-potential treatment of the semicore states is conceptually very easy within the KKR formalism.

As another example of our results, Fig. 3 shows the calculated volume changes per impurity in dilute Al-alloys with 3d and 4sp impurities [23]. With the exception of Mn the results are in a very good agreement with the lattice-parameter measurements [24]. Typically the 3d impurities show a large inward relaxation of the first nearest neighbors. For instance, for an Fe impurity the first nearest neighbors relax inward by 4 %, whereas in Cu the corresponding relaxation is practically zero. As a consequence in Al the local moments of the 3d impurities are strongly affected by the relaxations. In particular, the Fe-moment, calculated to be 1.5 μ_B in the ideal lattice geometry, vanishes in the relaxed configuration which is in agreement with susceptibility studies.

8.5 Calculation of Phonons

Many of the macroscopic properties of a crystalline material (e.g., specific heat, velocity of sound, thermal expansion) are determined by its vibrational degrees of freedom. The knowledge

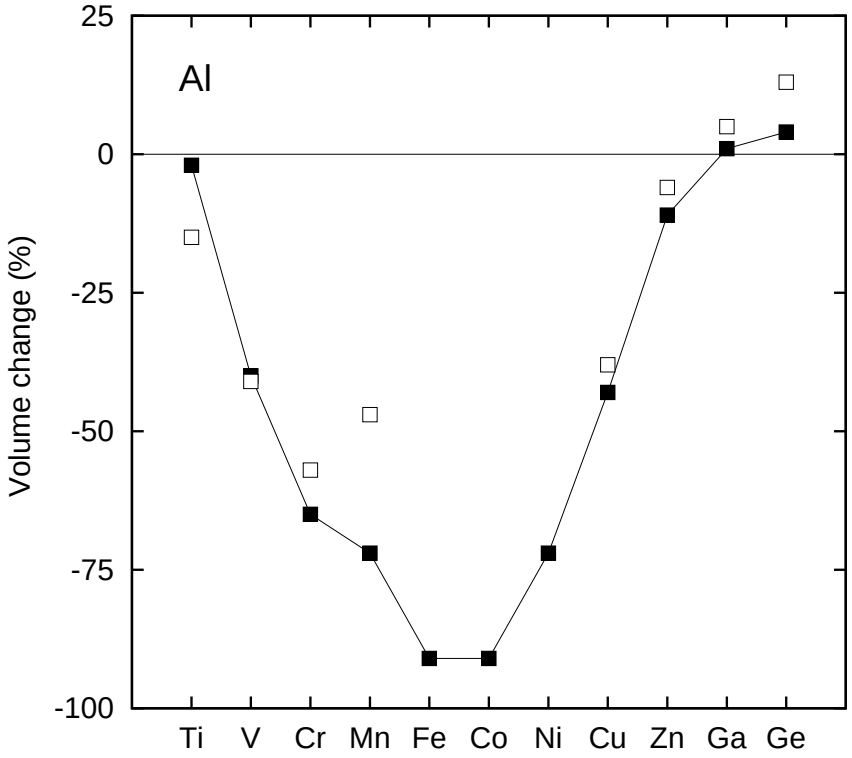

Figure 3: Calculated relative volume change per impurity in Al-based dilute alloys with 3d and 4sp impurities (filled squares). The results of lattice-parameter measurements [24] are also shown (empty squares).

of the phonon spectrum enables the calculation of the free energy within the quasi-harmonic approximation. The instabilities and peculiarities of the phonon spectrum may be used to understand phase transformations. Traditionally, phonon dispersion curves are calculated by lattice dynamics employing, e.g., the harmonic approximation, where one has to use some kind of analytical models for forces between atoms to obtain the force constant matrix. The first *ab initio* calculations for phonons in transition metals were performed using the frozen-phonon technique, where a (high symmetry) commensurable phonon **k**-vector is chosen and the atomic positions inside the corresponding supercell are displaced accordingly. From the calculated total energies one can then deduce the frequency of the chosen phonon mode. A recently introduced variational linear-response method avoids the use of supercells and can be applied to any phonon wave-vector [25]. For each **k**-value a new self-consistent calculation is required. In this highlight we show that the full-potential KKR-GF method can be used to determine the whole phonon spectrum of a transition metal from a single self-consistent calculation in real space.

We start from the definition of the Born-von Karman parameters Φ_{ij}^{mn} in the harmonic theory. By displacing the atom n in the direction j by the amount s_j^n, the force on the atom m in the direction i is given by $F_i^m = -\Phi_{ij}^{mn} s_j^n$. Thus we displace one atom by a small amount s_j^n in the ideal lattice and then calculate the forces F_i^m on all neighboring atoms self-consistently. This represents a typical "impurity problem" which can be handled by the above described full-potential KKR-GF method. For a cubic crystal with one atom per unit cell, only a single self-consistent calculation with a shift, e.g., in (100) direction, is sufficient to determine all non-equivalent Born-von Karman parameters Φ_{ij}^{mn}. The phonon frequencies for all **k**-vectors in the

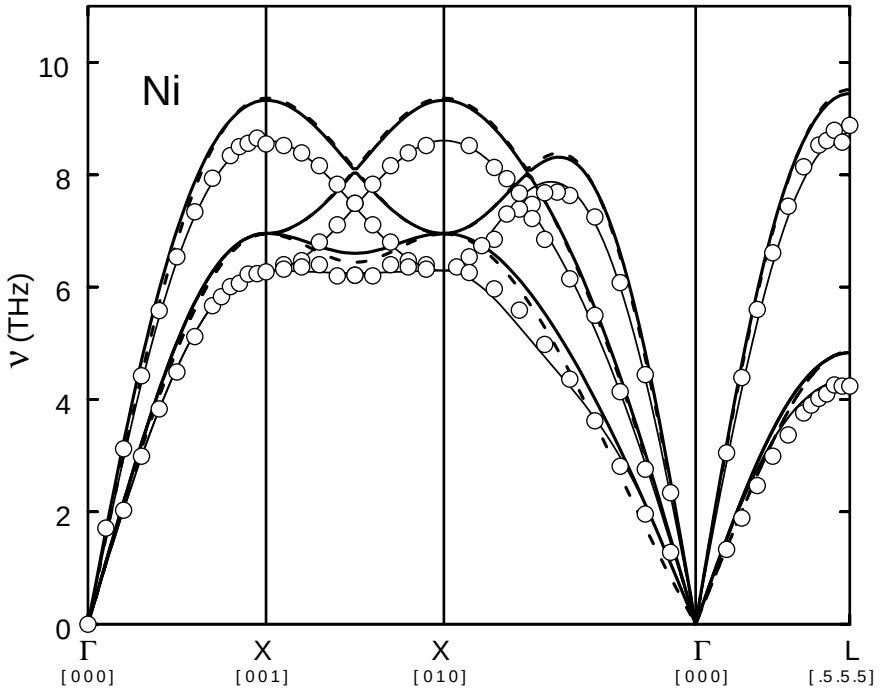

Figure 4: Calculated (solid line) and experimental (open circles) phonon spectra of fcc Ni. The phonon spectra obtained from a non-spin-polarized calculation is also shown (dashed line). The thin solid line is a Born-von Karman fit to the experimental points.

Brillouin zone can then be easily obtained by a Fourier transform. In the calculations below for fcc metals we use a displacement of 0.5 % of the NN distance and calculate the forces on 5 fcc shells of neighboring atoms. The effects of third order anharmonicities are corrected by symmetry considerations.

In Fig. 4 the calculated phonon dispersion curves of fcc nickel are compared with the experimental ones determined by neutron scattering. The overall agreement of the shape of the spectra is very good. The calculated phonon frequencies are slightly higher than the experimental ones, but this is probably due to the LDA used in the electronic structure calculation. The standard trend of the LDA is to make the lattice stiffer by reducing lattice constants by a few percent and by overestimating elastic constants. The calculated *ab initio* lattice constant for fcc Ni (6.52 a.u.) was used in the phonon calculations instead of the experimental value (6.65 a.u.). In Fig. 4 also the result of a non-spin-polarized calculation is shown by the dashed line. It is seen that the magnetism of Ni has not any remarkable effect on the phonon spectra, which one might anticipate since Ni does not undergo any structural phase transition between the low-temperature ferromagnetic and the high-temperature paramagnetic phases nor do the lattice parameter and the elastic constants show any significant anomalies near the Curie temperature. We have also calculated the phonon spectra of fcc Cu for different lattice parameter values and used these to determine the vibrational contribution to the lattice free energy. The lattice constant as a function of temperature was determined from these calculations and the thermal expansion coefficient of Cu was found to be $\alpha_{\rm theor} = 16 \cdot 10^{-6}$ K^{-1}, which is in surprisingly good agreement with the experimental value $\alpha_{\rm exp} = 17 \cdot 10^{-6}$ K^{-1}.

8.6 Summary and Outlook

We have demonstrated in this highlight that the full-potential KKR-Green's function method allows an efficient evaluation of forces and enables the study of lattice relaxations around impurities in metals, especially in transition metals where methods based on plane waves are difficult to apply. The forces are calculated by the ionic Hellmann-Feynman theorem and the Green's functions for shifted atomic positions are obtained by angular momentum transformations. It is also demonstrated how the whole phonon spectrum of a transition metal can be determined from a single self-consistent calculation in real space.

We have applied the full-potential KKR-GF method to predict impurity induced lattice relaxations around a large number of impurities in Cu (3d, 4sp, 4d, and 5sp impurities) and in Al (3d and 4sp impurities). The results for first NN displacements and macroscopic volume changes induced by impurities are in good agreement with the available experimental data from EXAFS and lattice parameter measurements. We have also used the method to calculate the phonon spectrum of ferromagnetic Ni and the thermal expansion coefficient of Cu. Both of these results are found to agree very well with experiments, the latter one even surprisingly well.

In the future we plan to implement force and relaxation calculations into our existing KKR-GF computer programs for surfaces, layered systems, and surface impurities. We believe that this can be done straightforwardly. We also want to point out that the described force and relaxation calculations can be used in connection with our recently developed version of the tight-binding KKR method [26, 27]. We are also developing a new method which allows to calculate bigger relaxations than the present version by reducing the angular momentum cut-off needed in the Dyson equation (14) at shifted positions. These improvements would make the KKR-GF formalism a very powerful tool to study the properties of materials from first principles.

Acknowledgments

This work has been supported by a bilateral German–Greek cooperation grant and was partially funded by the TMR Network "Ab initio calculations of magnetic properties of surfaces, interfaces and multilayers" (Contract: ERBFMRXCT960089). It has also benefited from collaborations within the HCM Network "Ab initio (from electronic structure) calculation of complex processes in materials" (Contract: ERBCHRXCT930369).

References

[1] J. Korringa, Physica **13**, 392 (1947).

[2] W. Kohn and N. Rostoker, Phys. Rev. **94**, 1111 (1954).

[3] Th. H. Dupree, Annals of Physics **15**, 63 (1961).

[4] J. L. Beeby, Prog. Roy. Soc. A **302**, 113 (1967).

[5] N. A. W. Holzwarth, Phys. Rev. B **11**, 3718 (1975).

[6] R. Zeller and P. H. Dederichs, Phys. Rev. Lett. **42**, 1713 (1979).

[7] R. Podloucky, R. Zeller, and P. H. Dederichs, Phys. Rev. B **22**, 5777 (1980).

[8] P. J. Braspenning, R. Zeller, A. Lodder, and P. H. Dederichs, Phys. Rev. B **29**, 703 (1984).

[9] I. Mertig, R. Zeller, and P. H. Dederichs, Phys. Rev. B **47**, 16 178 (1993).

[10] R. Zeller, J. Phys. C **20**, 2347 (1987).

[11] D. M. Nicholson and J. S. Faulkner, Phys. Rev. B **39**, 8187 (1989).

[12] A. Gonis, X.-G. Zhang, and D. M. Nicholson, Phys. Rev. B **40**, 947 (1989).

[13] J. Molenaar, J. Phys.: Cond. Mat. **1**, 6559 (1989).

[14] R. G. Brown and M. Ciftan, Phys. Rev. B **39**, 3543 (1989).

[15] E. Badralexe and A. J. Freeman, Phys. Rev. B **37**, 1067 (1988).

[16] R. G. Newton, Phys. Rev. Lett. **65**, 2031 (1990).

[17] B. Drittler, M. Weinert, R. Zeller, and P. H. Dederichs, Solid State Commun. **79**, 31 (1991).

[18] K. Wildberger, P. Lang, R. Zeller, and P. H. Dederichs, Phys. Rev. B **52**, 11 502 (1995).

[19] N. Papanikolaou, R. Zeller, P. H. Dederichs, and N. Stefanou, Phys. Rev. B **55**, 4157 (1997).

[20] A. Lodder, J. Phys. F **6**, 1885 (1976).

[21] G. Leibfried and N. Breuer, *Point Defects in Metals I* (Springer-Verlag, Berlin, 1978).

[22] U. Scheuer, B. Lengeler, Phys. Rev. B **44**, 9883 (1991).

[23] N. Papanikolaou, R. Zeller, P. H. Dederichs, and N. Stefanou, Comp. Mater. Sci. **8**, 131 (1997).

[24] H. W. King, J. Mater. Sci. **1**, 79 (1966).

[25] S. Baroni, P. Giannozzi, and A. Testa, Phys. Rev. Lett. **58**, 1861 (1987).

[26] R. Zeller, Phys. Rev. B **55**, 9400 (1997).

[27] K. Wildberger, R. Zeller, and P. H. Dederichs, Phys. Rev. B **55**, 10 074 (1997).